THESIS

SKILLFUL LONG-RANGE FORECASTS OF NORTH AMERICAN HEAT WAVES FROM PACIFIC STORM PROPAGATION

Submitted by

Andrea Jenney

Department of Atmospheric Science

In partial fulfillment of the requirements

For the Degree of Master of Science

Colorado State University

Fort Collins, Colorado

Summer 2017

Master's Committee:

Advisor: David Randall

Elizabeth Barnes
Georgiana Brooke Anderson

ABSTRACT

SKILLFUL LONG-RANGE FORECASTS OF NORTH AMERICAN HEAT WAVES FROM PACIFIC STORM PROPAGATION

Extreme heat poses major threats to public health and the economy. Long-range predictions of heat waves offer little improvement over climatology despite the continuing improvements of weather forecast models. Previous studies have hinted at possible relationships between tropical West Pacific convection and subsequent anomalous near-surface air temperature and rainfall over the North American Plains. We show that the later stages of propagation of the Boreal Summer Intraseasonal Oscillation (BSISO) can be used to skillfully hindcast a number of Great Plains heat waves between 1948 and 2016 with a three-month lead time. Possible teleconnection mechanisms are investigated, with no mechanism appearing more likely. Our results are the first to demonstrate that a West Pacific weather event can be used to skillfully forecast US Plains heat waves with a lead time of three months.

ACKNOWLEDGEMENTS

I would like to acknowledge the immensely helpful scientific counsel given to me by Karen McKinnon, post-doctoral fellow at the National Center for Atmospheric Research in Boulder, Colorado. Karen also provided much of the inspiration for and computer code used in this project—possibly speeding up the completion of this project by a year or more.

This work has been supported by the National Science Foundation Science and Technology Center for Multi-Scale Modeling of Atmospheric Processes, managed by Colorado State University under cooperative agreement No. ATM-0425247.

TABLE OF CONTENTS

CHAPTER 1—INTRODUCTION

The adverse health outcomes due to exposure to extreme heat have been thoroughly documented [*Portier et al.*, 2010]. The United States (US) Great Plains is a particularly sensitive region, where evapotranspiration by plants exceeds precipitation, making the region especially prone to drought [*Melillo et al.*, 2014], and thus heat waves through soil moisture-precipitation feedbacks and the association of near-surface air temperature with soil moisture [*Eltahir*, 1998; *Koster et al.*, 2004]. More accurate forecasts of heat waves would enable better preparation, which could alleviate some of their human and economic tolls. Unfortunately, state-of-the-art numerical predictions of extreme heat struggle to offer much improvement over climatology [*Luo and Zhang*, 2012].

There has been some success in statistical forecasting of weather events using the observed relationships between intraseasonally varying climate phenomena and a target predictand [e.g. *Barnston*, 1994; *Drosdowsky and Chambers*, 2001; *Slade and Maloney*, 2013; *McKinnon et al.*, 2016]. Convective variability in the Indian Ocean/West Pacific region has been shown excite teleconnections that affect weather in the extratropics [*Hoskins and Karoly*, 1981; *Ferranti et al.*, 1990; *Donald et al.*, 2006]. However, a causal link between this convection and US summer heat waves has not yet been identified. The boreal summer intraseasonal oscillation (BSISO) is a complex,

leading mode of intraseasonal convective variability in the Indian Ocean-West Pacific region [*Yasunari*, 1979; *Lau and Chan*, 1986; *Wang and Rui*, 1990; *Wang and Xie*, 1997], that has previously been linked with North American fluctuations of surface air temperature and precipitation [*Moon et al.*, 2013]. Here, we test whether the BSISO can be used as a predictor of US heat waves.

We confine our analysis of spring BSISO propagation to May and of summer heat waves to August. Extending the analysis to include other spring and summer months severely weakens forecast skill. This may be due to the sensitivity of the teleconnection response to the seasonal cycle of the atmosphere's background state; previous work has suggested that North American weather responds most readily to low-frequency forcing from the West Pacific (e.g., the BSISO) given the spring-time configuration of the mean circulation over the Pacific [*Newman and Sardeshmukh*, 1998]. A possible additional factor is the seasonality of the BSISO itself, which occurs from May to October [*Wang and Rui*, 1990] but changes significantly between the beginning and end of summer [*Kemball-Cook and Wang*, 2001].

CHAPTER 2—METHODS

2.1 Data

Daily maximum temperature observations are from Global Historical Climatology Network-Daily [*Menne et al.*, 2012]. We use weather station data, instead of a gridded reanalysis product, because values represent actual in-situ measurements, instead of smoothed model output.

We identify the BSISO using outgoing longwave radiation (OLR) and 850 hPa zonal wind from the NCEP/NCAR Reanalysis 1 [*Kalnay et al.*, 1996]. Four-times daily values of the OLR are averaged to daily means and then re-gridded, using bilinear interpolation, to the same grid (2.5° x 2.5°) used for the zonal wind data. We use this reanalysis dataset because it extends further back in time (1948) than newer reanalysis products, thus allowing identification of a larger sample of heat waves, which are rare events. Because of the limited accuracy of OLR from reanalysis datasets, we repeat the analysis with BSISO indices [*Lee et al.*, 2013] that use an OLR product measured from satellites (Advanced Very High Resolution Radiometer [*Liebmann and Smith*, 1996]) and a newer reanalysis product for zonal wind (NCEP-DOE Reanalysis 2 [*Kanamitsu et al.*, 2002]). Despite some differences in skill and the number of heat waves correctly forecast, forecasts made from BSISO indices that use satellite data and a newer

reanalysis dataset still give a significant ($p < 0.01$ for BAT = 0.0 to 0.7) increase in forecast skill relative to climatology (see Figure A.1).

Geopotential height data at 200 and 500 hPa are from the NCEP/NCAR Reanalysis 1 [*Kalnay et al.*, 1996]. For all data hitherto described, anomalies are constructed by removing the long-term mean and the first three annual harmonics.

Daily rainfall data is from the Climate Prediction Center unified gauge-based analysis of daily precipitation [*Chen et al.* 2008]. We use the standardized precipitation index (SPI) [*McKee et al.*, 1993] to diagnose integrated anomalous precipitation. Rainfall is highly spatially inhomogeneous, and fits more closely to a gamma distribution than a Gaussian. The SPI is thus useful because it presents accumulated rainfall anomalies as standardized departures from a climatological mean. We use an accumulation period of 60 days as a proxy for soil moisture, and of 15 days to diagnose late-spring precipitation anomalies prior to August heat waves.

2.2 Defining BSISO phases

A previous study defined a BSISO index using the leading two empirical orthogonal functions (EOFs) of anomalous daily OLR and zonal wind at 850 hPa for the region 10°S-40°N, 40°-160°E [*Lee et al.*, 2013]. To construct a principal component (PC) time series for the time period being evaluated (1948-2016), we project daily anomalies of the same variables onto these aforementioned EOFs. Anomalies are constructed as described previously, except that we also subtract the running mean of

the previous 120 days to remove any long-term variability or trends [*Wheeler and Hendon*, 2004]. The daily two-dimensional standardized phase space defined by the two PCs can be used to diagnose the BSISO phase (see Figure 3c for an example) [*Lee et al.*, 2013; *Wheeler and Hendon*, 2004]. BSISO amplitude, defined as the square root of the sum of each squared, standardized PC, quantifies the degree to which that day's pattern in OLR and zonal wind resemble the idealized pattern defined by the phase.

2.3 BSISO propagation

We identify unique spring BSISO propagation events as time periods for which there is progression from either Phase 4 to 7 or Phase 5 to 8 (the events that progress from Phase 4 to 8 are counted only once), with the additional requirement that the first day of the progression is in May (see Figure 1 for a physical representation of BSISO phases). Progression must occur within 30 days or less from the first day of the starting phase, and movement two phases forward or backward is permitted. It is useful to classify propagation events using a BSISO amplitude threshold (BAT), such that low-amplitude events are excluded from the analysis. For each BAT considered, forecasts are made requiring that at a given BAT, at least half of the days during the propagation exceed that amplitude. Propagation through consecutive, monotonically increasing BSISO phases does not happen often in our data. Thus, restricting propagation to only allow for backwards movement in phase value by one or not at all reduces the number of spring propagating BSISO events in our sample (for example, at a BAT of one, we

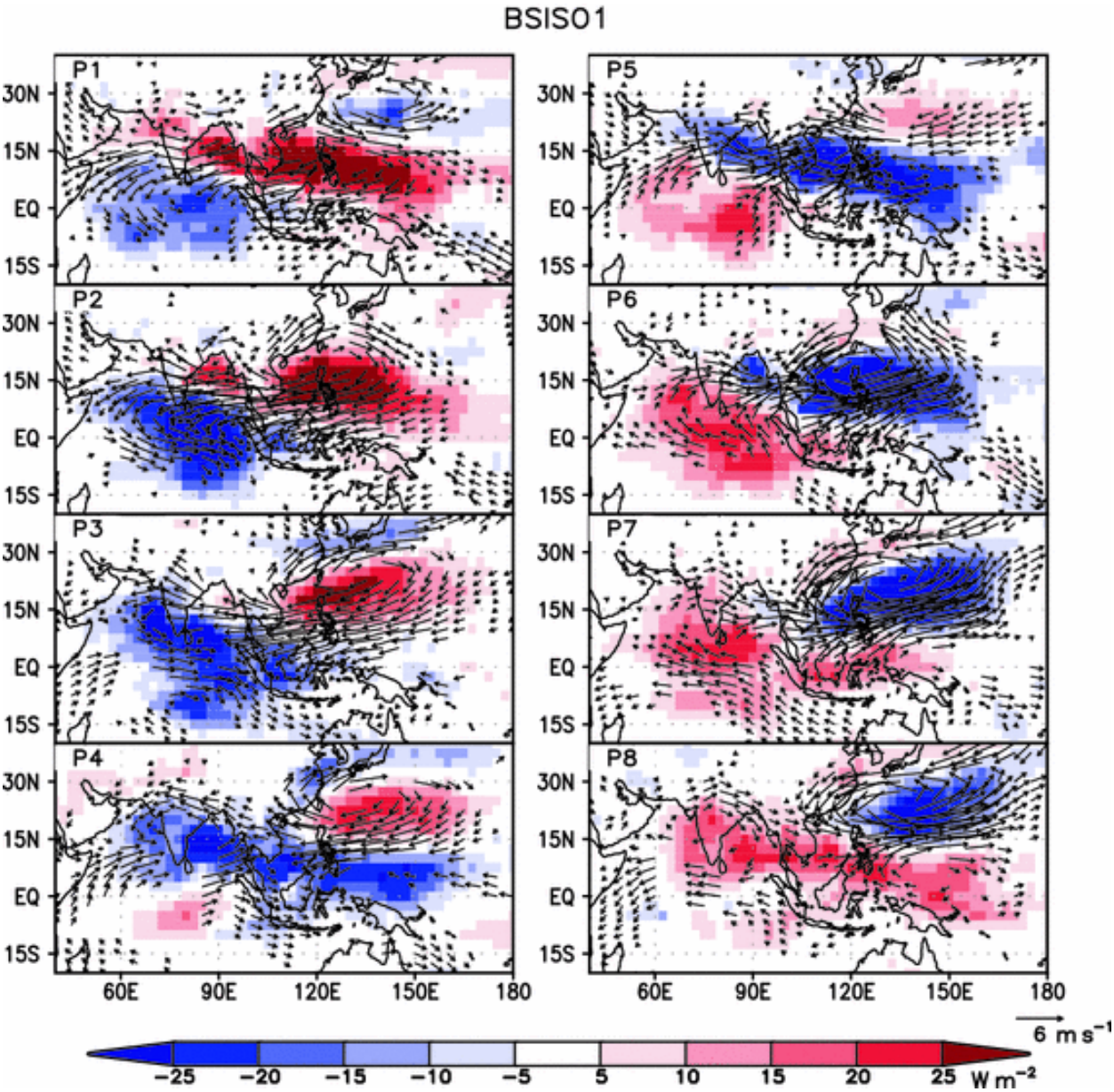

Figure 1: Outgoing longwave radiation (shading) and 850 hPa wind (vectors) for BSISO indices. From Lee et al. (2013).

identify 36 events when allowing for jumps in phase value by two, but only 17 when requiring that phase propagation only be forward in increments of one).

In hindcasts, lags in time are counted from each day of the fourth phase in the propagation (e.g., each occurrence of Phase 7 if propagation began at Phase 4). A

correct forecast is counted when there is a heat wave day exactly N_{lead} days later (here, we present skill for forecasts made for a lead time of N_{lead} equal to 80 days; see Figure A.2 for skill for lead times between 70 and 90 days). For example, for a spring BSISO propagation event where the last phase has multiple days of occurrence, each of those days that is followed by a heat wave day exactly N_{lead} days later is counted towards the true positive rate. The true positive rate is the number of correct forecasts divided by the total number of spring days that are the fourth phase of propagation.

Despite the long lead times, we use a window of exactly one day for forecasts rather than a larger window of a few days. This is because of the large amount of memory both in heat waves and in BSISO propagation. That is, we use consecutive days of May BSISO Phase 7 or Phase 8 to forecast heat wave days, which are also by definition consecutive. This, combined with the short window of time for which forecasts can be made (the month of August), and the fact that our heat wave definition identifies heat waves in most Augusts during the time period being analyzed (44 of 69 years), makes the likelihood of a correct forecast by chance very high when using a window longer than a day. For heat wave forecasts, we compare skill to the climatological rate of August heat wave days, which is equivalent to the likelihood of a correct forecast by chance when using a window of one day.

2.4 Defining heat waves

Following a previous study [*McKinnon et al.*, 2016], only weather stations that have data for at least 70% of June, July, and August for at least 70% of the years considered (1948-2016) are chosen for the analysis. For the Plains region, 414 weather stations satisfy this requirement. We define heat waves as two or more consecutive hot days, where hot days are those for which the spatial 95th percentile [*McKinnon et al.*, 2016] of temperature anomalies in the Plains domain is larger than 7.5°C. We choose this definition because it gives a climatological rate of August heat waves of about 13%, a rate small enough so that they qualify as rare events, but large enough to give enough heat waves during the 69-year record (1948 to 2016) to yield reliable statistics. Hot days that occur less than two days after a heat wave, and the days in between, are counted as part of the heat wave. With this definition, we identify 72 August heat waves, with a median event duration of 3 days.

2.5 CGT index

Following a previous study [*Ding and Wang,* 2005] we create a circumglobal teleconnection (CGT) index (CGTi) using summer seasonal mean (June through September) anomalies of 200 hPa geopotential heights over the Northern Hemisphere (0° to 90°N), which are monthly averaged from daily anomalies and then averaged for the summer season. Figure 2 shows the second EOF of these heights, which represents the spatial CGT pattern [*Ding and Wang,* 2005]. The PC time series is constructed by

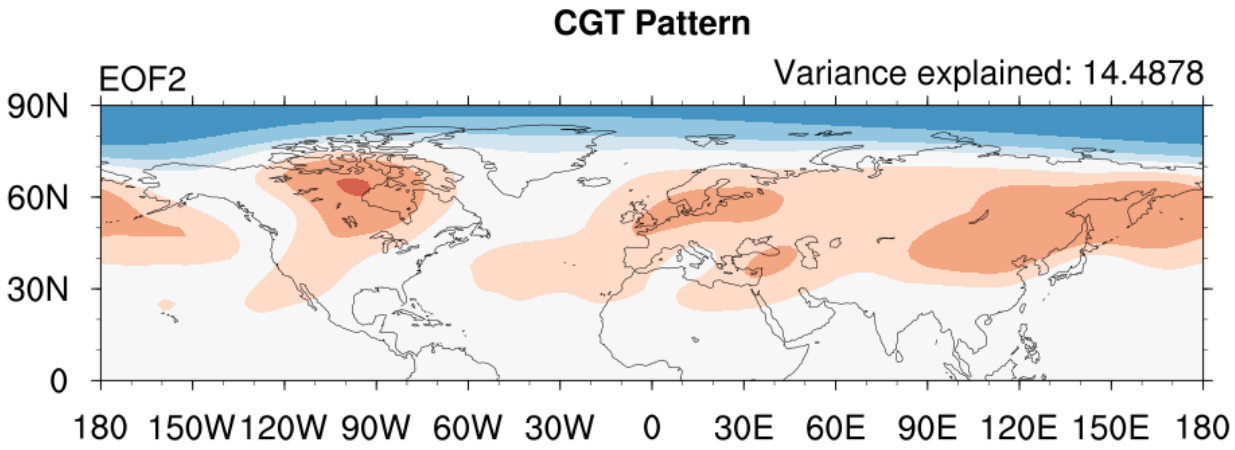

Figure 2: Circumglobal teleconnection (CGT) pattern, shown as the second empirical orthogonal function (EOF2) of seasonal (JJAS) mean 200 hPa heights from 1948-2016.

projecting band pass filtered, daily anomalies of Northern Hemisphere 200 hPa geopotential height onto this EOF pattern. In filtering, we use two moving average boxcar windows of 11 days and 365 days: We first remove high frequencies by creating a lowpass filtered time series using a window of 11 days (T1), and then remove low frequencies by subtracting from T1 the time series constructed using a window of 365 days on T1. Standardization of the resulting time series gives the CGTi used here.

2.6 Statistics

For all significance tests, we use bootstrapping with 10,000 samples. We use a one-tailed block bootstrap to test the significance of heat wave forecasts after BSISO propagation. To do this, we randomly select from all Mays N_{BAT} blocks of length X_{BAT} consecutive days and forecast heat waves as described previously for each of these $N_{BAT} \times X_{BAT}$ May days. N_{BAT} is the number of spring BSISO propagation events and X_{BAT} is the integer-rounded average number of forecast-used days (i.e., consecutive

instances of Phase 7 or Phase 8) contained within each propagation event for each BAT. Significance of forecast skill is tested at the 99% confidence level. We use a two-tailed, classic bootstrap test at the 95% confidence level for all other significance tests. For these tests, we are randomly sampling years within our data's time domain (1948-2016).

CHAPTER 3—BSISO-BASED FORECASTS OF PLAINS HEAT WAVES

BSISO phases are defined using anomalies of OLR and zonal wind at 850 hPa over the Indian Ocean/West Pacific region [*Lee et al.*, 2013]. Each day can be given a phase value between 1 and 8 and an amplitude (see methods). The phase value is indicative of the general location of convection (see Figure 1): Phase 1 convective centers are in the equatorial Indian Ocean and slowly propagate northeastward in a northwest-southeast tilted band through later phases until Phase 8 (after about 30-60 days), where convective centers reach the subtropical West Pacific [*Lee et al.*, 2013].

Composites of high-amplitude BSISO phases (those with BATs greater than 1.5, see methods) prior to August Plains heat waves reveal a preferred pattern of propagation from Phase 4 to Phase 8 roughly 100 to 80 days prior to the heat wave (Figure 3). While the distribution of BSISO phases 100 to 80 days prior to non-heat wave August days (Figure 3b) is generally uniform (with some preference for Phases 6 through 8), that for heat waves (Figure 3a) has an increased representation of Phases 4 and 5 for earlier lags (100 to 96 days), and a transition to an increased representation of Phases 7 and 8 for later lags (85 to 81 days). This transition suggests that the BSISO is propagating from Phases 4 and 5 to Phases 7 and 8 in the 100 to 80 days prior to August Plains heat waves. Physically (see Figure 1), this manifests as convective activity oriented along a large northwest-southeast band extending from India to the West

Pacific Ocean just north of Papua New Guinea during BSISO Phase 4. This band migrates northeastward in Phase 5, and becomes a zonally extended (between about 100° to 160°E) cyclone at about 15°N in the West Pacific by Phase 6. The cyclone moves further northeastward by Phases 7 and 8, and shrinks in its zonal extent in Phase 8.

Averages of the PCs used to identify BSISO phases (see methods) between 120 and 80 days prior to heat waves, for days where the standardized PCs exceed 1.06 (equivalent to a BSISO amplitude of 1.5), similarly reveal this preferred pattern of propagation through the later phases of the BSISO (Figure 3c). Henceforth, we refer to BSISO propagation as progression through four BSISO phases, counting from the first May instance of either Phase 4 or 5 (see methods).

Using the observed pattern of BSISO propagation as a heat wave predictor, we show significant ($p = 0.00005$) improvement in eighty-day nonprobabilistic (yes/no) heat wave day forecasts relative to those based on climatology. The darker values (numbers indicate the number of unique heat waves correctly forecast) in Figure 4 show the true positive rate (ratio of hits to sum of hits and false alarms, considering individual days rather than entire heat wave events) of heat wave day forecasts as a function of the BSISO amplitude threshold (BAT, see methods). At low BATs, 12 of the 72 August Plains heat wave events (event hit rate of 16.7%) were correctly forecast, with a true positive rate of 26%, a 13% improvement over climatology. Forecast skill generally

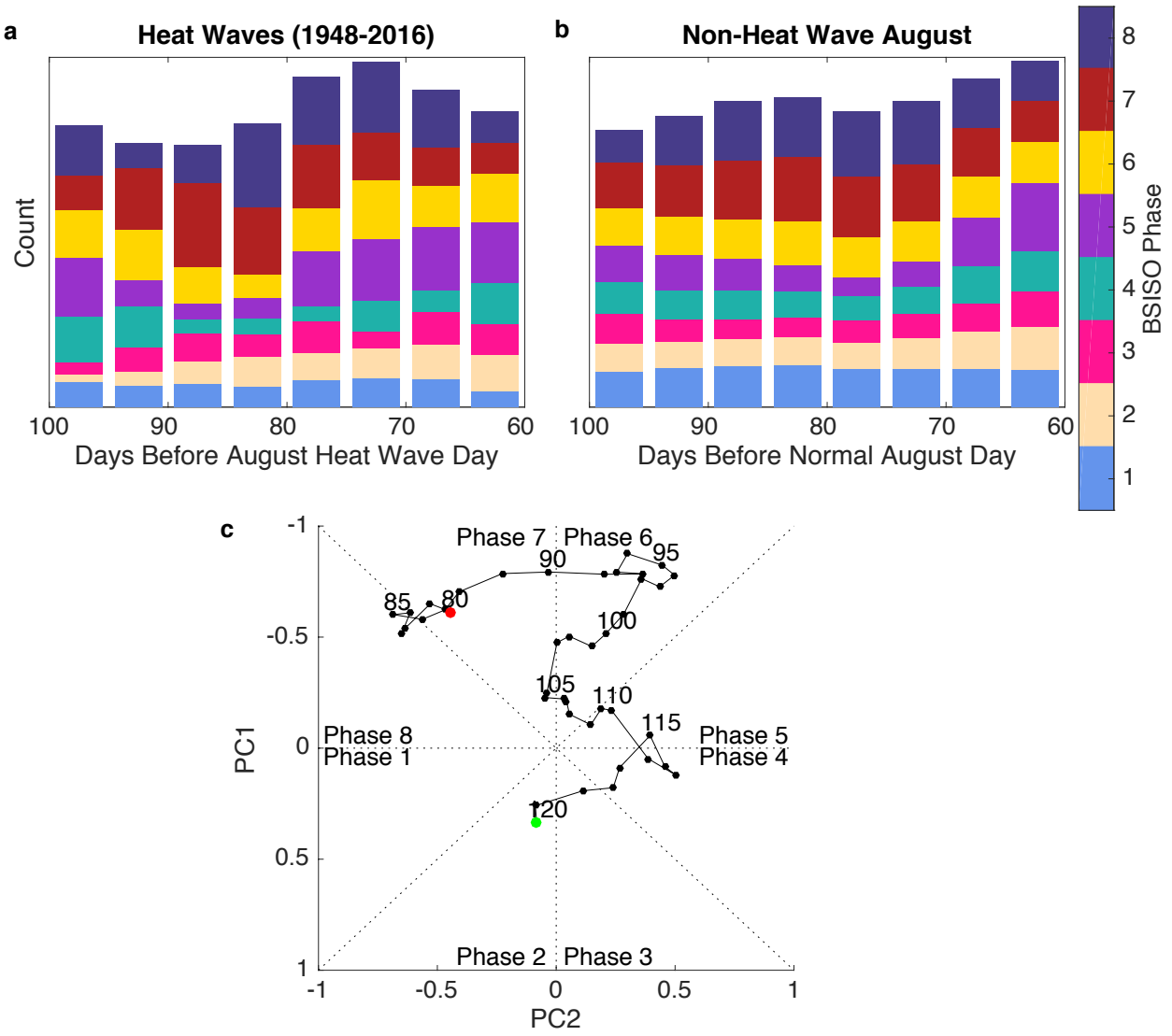

Figure 3: **a,** Composites of BSISO phases prior to August Plains heat waves and **b,** non-heat wave August days between 100 and 60 days prior to the August day. Only days with amplitudes exceeding 1.5 are included. **c,** Composite BSISO phase space 120 to 80 days prior to August Plains heat waves. Only days where the standardized principal component (PC) amplitudes exceeds 1.06 (roughly equivalent to a phase amplitude of 1.5) are included.

increases with BAT for BATs larger than 1.5; however, the concurrent sharp decrease in sample size implies that this apparent increase in skill, although significant, should be viewed with caution. Forecasts are made for a lead time of exactly 80 days. However,

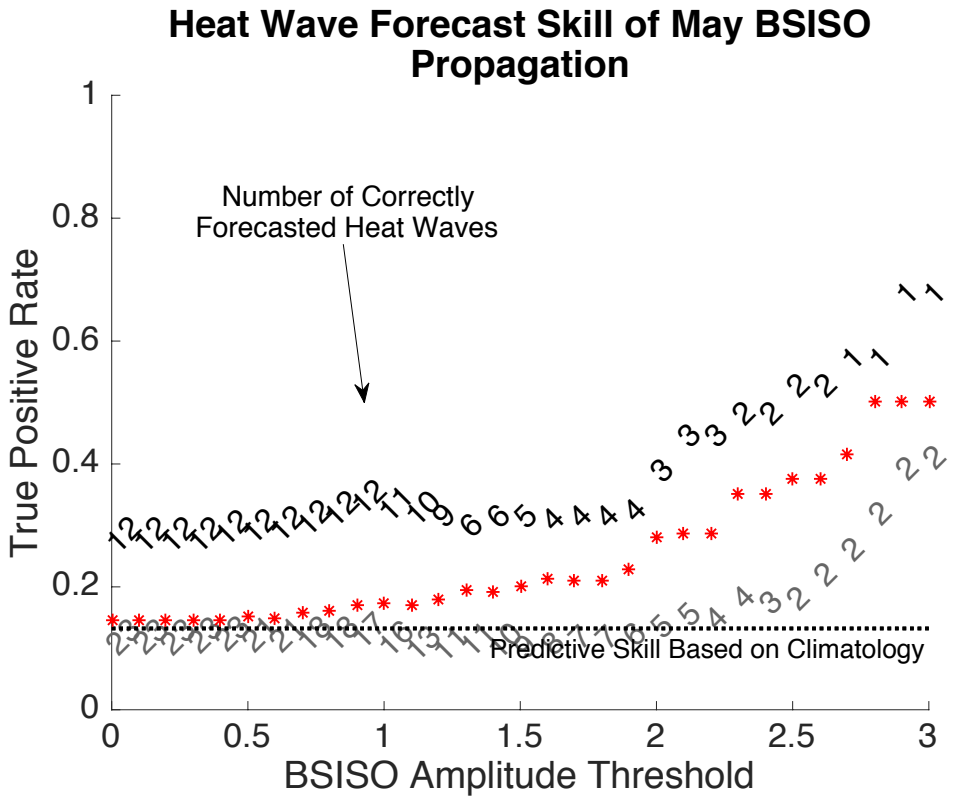

Figure 4: Skill of May BSISO propagation in predicting August Plains heat wave days. Vertical position shows skill in true positive rate (proportion of May days that predict a heat wave day 80 days later) for BSISO Phases 7 and 8 (grey numbers), and for BSISO Phases 7 and 8 that are preceded by BSISO propagation (black numbers). Skill is shown as a function of the BSISO amplitude threshold. Black dotted line is the climatological rate of August heat waves, and red asterisks indicate forecast skill significance at 99% confidence computed using a block bootstrap. Numbers indicate the number of unique heat wave events correctly forecast.

skill remains significant for BATs up to 1 ($p < 0.01$) for forecasts made with lead times between 78 and 87 days (see Figure A.2 and Table A.1.) Both skill and the number of heat waves correctly forecasted peak for a lag of 80.

These forecasts are made from each daily instance of the end phase of BSISO propagation (i.e., each successive day classified as either Phase 7 or 8). Relaxing the forecast metric to include also those spring Phase 7 and 8 days not preceded by BSISO

propagation drastically weakens the forecast skill, offering no improvement over forecasts based on climatology (grey numbers in Figure 4). This suggests that BSISO propagation, rather than a West Pacific convective pattern that happens to look like a BSISO Phase 7 or 8, is essential to the chain of events that leads to heat waves roughly 80 days later.

To test whether our results are sensitive to the definition of heat waves, we repeat the analysis from the previous section but now define hot days as those where at least 20% of the Plains experiences a maximum daily temperature of at least 35°C (95°F). Station temperatures are now the actual temperatures reported at each location, rather than filtered anomalies where seasonality has been removed. We choose 20% because it produces a climatological heat wave rate of 14%, which is close to the climatological rate obtained with the previous definition. We identify 76 August heat waves between 1948-2016 with a median duration of 3 days. Forecasts of these heat waves using the metric previously described have almost identical skill to those made with the previous heat wave definition (see Figure A.3). BSISO propagation forecasts 11 of these 76 heat waves (an event hit rate of 14%). Additionally, there is substantial overlap in the heat wave events correctly forecast between the two definitions (10 out of the 11 events forecast with this definition were also forecast with the previous definition). Thus, statistical heat wave forecasts using BSISO propagation as the forecast metric are not sensitive to the specific way a heat wave is defined.

Thus far, we have shown that a number of August Plains heat waves can be skillfully forecast using propagation of a West Pacific storm pattern—the BSISO—with a three-month lead time. However, the physical mechanisms controlling this teleconnection are still unclear. In the following chapter, we explore some possible atmospheric and oceanic systems that could be physically connecting spring BSISO propagation to summer Plains heat waves, either directly, or as a third-party driver of both phenomena.

CHAPTER 4—TELECONNECTION MECHANISMS

A three-month lead time is implausible for a teleconnection communicated solely through the rapidly-varying and chaotic troposphere. This suggests that the "memory" of BSISO propagation is held in some form other than a tropospheric mode of variability. Here, we consider some possible teleconnection mechanisms involving slowly-varying systems: the El Niño Southern Oscillation (ENSO), a soil moisture-precipitation feedback, and an actively-participating extratropical Pacific ocean. We also suggest a possible teleconnection through a low-frequency mode of summer circulation variability.

4.1 El Niño

ENSO is known to influence forecast skill in seasonal prediction models [*Pepler et al.*, 2015]. In addition, previous work has shown that interannual variability of the BSISO is tied to ENSO [*Teng and Wang*, 2003; *Lin and Li*, 2008]. That is, during the El Niño-developing (decaying) summer, BSISO propagation is enhanced (weakened) [*Lin and Li*, 2008]. ENSO could modulate our heat-wave forecast skill by acting as a third-party amplifier of both BSISO propagation and August mean temperature, and/or through regulation of the BSISO-heat wave teleconnection. We use the January Niño 3.4 index [*Trenberth*, 1997] as an indicator of the ENSO-decaying mode. A positive (negative) January Niño 3.4 index would indicate an El Niño (La Niña)-decaying year.

We reject the former possibility because we find no significant difference between August mean temperatures for years with and without detected BSISO propagation (mean p = 0.23 for BATs from 0 to 1), and also because we find that the proportion of years with BSISO propagation that also have heat waves is the same or less than the proportion of all domain years with heat waves in the Plains region (see Figure A.4). In addition, we find that the mean January Niño 3.4 indices do not differ between years with and without Plains heat waves (p = 0.11). This further supports the notion that May BSISO propagation is a causal precursor to the predicted August heat waves.

We do find some evidence that ENSO may be modulating the BSISO-heat wave teleconnection by influencing the interannual variability of BSISO propagation. Previous studies suggest that BSISO intensity is weaker in El Niño-decaying summers [*Lin and Li*, 2008]; however, we find that the mean January Niño 3.4 index for years where our algorithm detects May BSISO propagation is significantly higher than for years with no detected propagation, indicating that May propagation is favored in El Niño-decaying years (p = 0.01). This is not necessarily in disagreement with previous studies that focus on BSISO intensity (amplitude, here); we simply find that May propagation through later phases of the BSISO is favored in El Niño-decaying years. Although we do find that the mean Niño 3.4 index is larger for years where BSISO propagation predicts heat waves than for years where BSISO propagation fails to predict heat waves, this difference is not significant (p = 0.09). Thus, on the basis of the

evidence at hand, we cannot reject the possibility that the BSISO has greater influence on Plains heat waves in El Niño-decaying years than in other years.

4.2 Soil Moisture Feedbacks

In the US Great Plains, coupling is strong between local precipitation and soil moisture in summer [*Koster et al.*, 2004] and between spring precipitation and subsequent summer precipitation [*Duerinck et al.*, 2016]. Additionally, soil moisture is understood to influence near-surface air temperature by regulating the partitioning between surface and latent heat fluxes [*Eltahir*, 1998]. When there is little soil moisture to support evapotranspiration, the energy of the absorbed solar radiation is returned to the atmosphere primarily as sensible rather than latent heat. The reduced evapotranspiration leads to less rainfall, and increased near-surface air temperatures. In this way, a dry spring can lead to a hot, dry summer.

Here we use the standardized precipitation index [*McKee et al.*, 1993] (SPI) with an accumulation period of 15 days (SPI-15) to show short-term accumulated rainfall anomalies, and with an accumulation period of 60 days (SPI-60) as a proxy for soil moisture (see methods). Figure 5 shows composites of 500 hPa geopotential height anomalies averaged over a 15-day period 84 to 70 days prior to correctly forecasted heat waves, SPI-15 based on the same 15-day period, and SPI-60 based on the 60 days prior to the heat waves. All fields have been averaged first over all days within a heat wave event and then composited over heat waves so as not to give more weight to

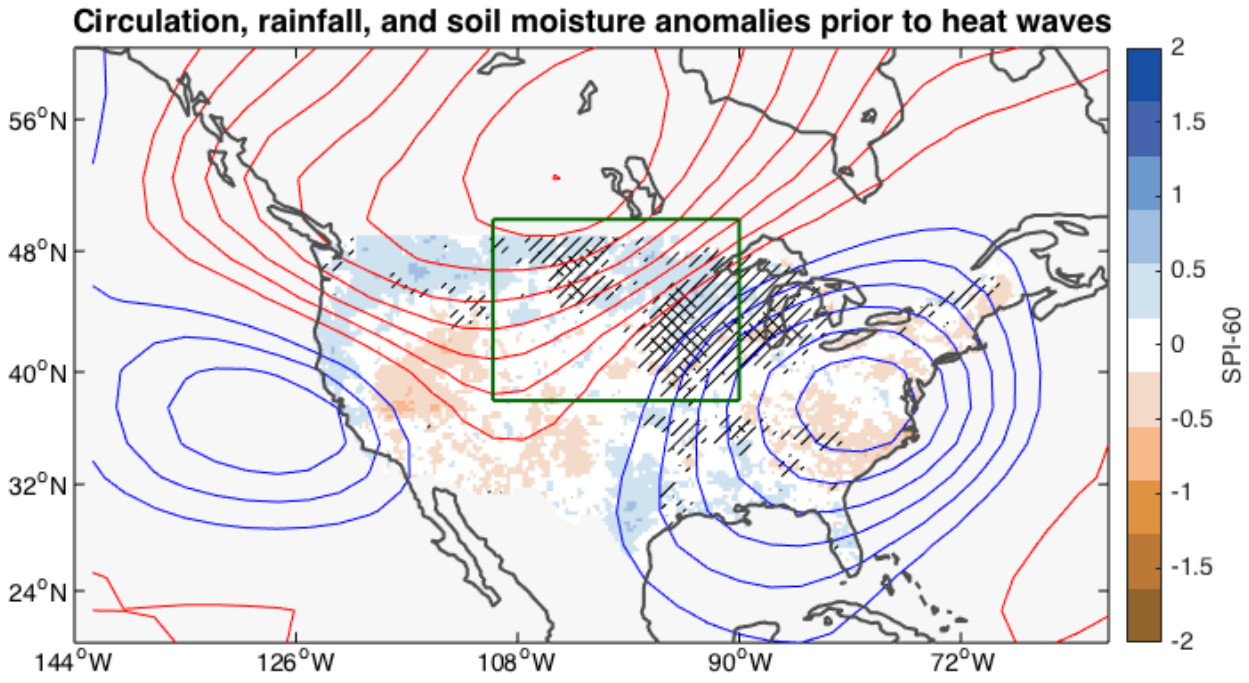

Figure 5: Composited geopotential height anomalies at 500 hPa (red: positive, blue: negative; increments of 5 m, beginning at 5 m) averaged over a 15-day period 84 to 70 days prior to heat waves, 15-day standardized precipitation index (SPI, black hatching; single hatch < -0.25, double hatch < -0.50) at 70 days prior to correctly forecasted heat waves, and 60-day SPI at the time of heat waves. Composites are averaged first over all days within the heat wave event, and then between each event, so as not to give more weight to heat waves longer in duration. The green square encloses the Plains region.

heat waves of longer duration; averaging over all heat wave days would disproportionally highlight the fields unique to longer heat wave events, whereas we are interested in characteristics shared by all correctly forecasted heat waves. The composite suggests that for correctly forecasted events, there appears to be a relationship between a blocking high and low spring rainfall. However, this is not collocated with dry summer soils at the time of the heat waves. Additionally, examination of the same fields for individual correctly forecasted events (Figure A.5)

reveals a high amount of variability in each of these fields and no event-to-event systematic patterns. Thus, there does not appear to be strong evidence that Plains soils retain the memory of spring BSISO propagation in a way that favors August heat waves, providing evidence against a soil moisture mechanism.

4.3 Pacific Ocean

Ocean temperatures exert a global influence on the atmosphere [*Ropelewski and Halpert*, 1987]. Previous studies have shown an association of the extratropical Pacific sea surface temperature (SST) with the summer large-scale atmospheric circulation [*Liu et al.*, 2006; *Frankignoul and Sennéchael*, 2007] and Great Plains drought [*Namias*, 1982]. One particular Pacific SST pattern has even recently been shown to skillfully predict heat waves in the Eastern US [*McKinnon et al.*, 2016]. These studies suggest that it is possible that the extratropical Pacific SSTs act as an intermediary between the BSISO and the Plains heat waves. Although not explored further here, it is possible that the ocean sea surface temperatures retain the memory of BSISO propagation and play an active role in the chain of events eventually leading to August Plains heat waves.

4.4 Circumglobal Teleconnection

The circumglobal teleconnection pattern (CGT) is a boreal summer low-frequency wavenumber-5 mode of the extratropical Northern Hemisphere circulation, and has a positive center located over high latitudes of North America (see Figure 2)

[*Ding and Wang, 2005]*. Additionally, the CGT is believed to be strongly influenced by variable heating in the South Asian region [*Ding and Wang, 2005]*. Thus, due to the quasi-stationary nature of the CGT, it is possible that BSISO propagation is linked to Plains heat waves through excitation of the CGT to produce a persistent summer high pressure system that extends over the Plains region and suppresses local precipitation. Land-atmosphere feedbacks may then come into play. Figure 6 shows the composited CGTi (see methods) prior to the first day of correctly forecasted heat waves. A positive (negative) CGTi here denotes high (low) geopotential heights over North America and the four other centers of action associated with this pattern. A CGTi close to zero indicates that there is no correlation between the day's geopotential height pattern and that of the CGT EOF. Here, we see that from about 90 days prior to the start of forecasted heat waves, the CGTi is only slightly positive. Inspection of the CGTi for individual heat waves reveals that it varies considerably between events, and does not appear to have any consistent, systematic behavior prior to correctly forecasted heat waves. We conclude that the CGT is unlikely to be involved in the teleconnection between May BSISO propagation and August Plains heat waves.

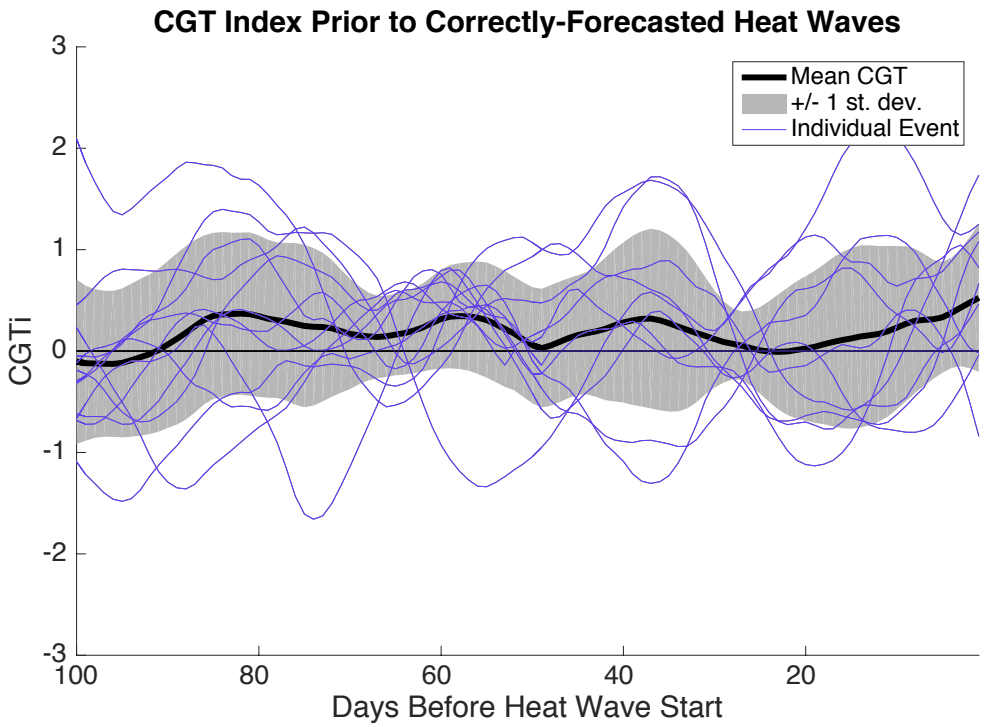

Figure 6: Circumglobal teleconnection (CGT) index (CGTi) prior to composited correctly forecasted heat waves (thick black line), +/- 1 standard deviation (grey shading), and for individual events (thin blue lines).

CHAPTER 5—CONCLUSIONS

The results presented here utilize a previously suggested link between West Pacific convection and North American temperature and rainfall anomalies [*Moon et al.*, 2013] to skillfully forecast Plains heat waves with a three-month lead time (see Figure 4). May propagation through the later phases [*Lee et al.*, 2013] of the BSISO a leading mode of boreal summer convective variability in the Indian Ocean/West Pacific region [*Yasunari*, 1979; *Lau and Chan*, 1986; *Wang and Rui*, 1990; *Wang and Xie*, 1997], is used to hindcast August Plains heat waves with a roughly eighty-day lead time. During this BSISO propagation, convective activity begins in a northwest-southeast tilted band extending from India to the West Pacific, just north of Papua New Guinea. The convection migrates northeastward and becomes associated with a large cyclone in the subtropical Western Pacific (see Figure 1).

Our results suggest that the BSISO-Plains heat wave teleconnection is direct, rather than the result of a third-party driver of both phenomena, because we obtain an increase in forecast skill when we make the predictor (May BSISO Phases 7 and 8) more discriminating by requiring that these days be preceded by BSISO propagation. Additionally, we do not find a significant difference between August mean temperatures for years with and without BSISO propagation. This is evidence against a third-party amplifier of both BSISO propagation and August heat.

Nonetheless, we do not find any strong evidence for a single physical mechanism linking BSISO propagation to Plains August heat waves. We looked for evidence that the memory of BSISO propagation is held in the land surface. However, there does not appear to be any systematic drying of summer Plains soils due to a spring BSISO teleconnection that causes decreases in spring rainfall.

We also looked for pre-heat wave systematic changes in the circumglobal teleconnection, a boreal summer quasi-stationary mode of Northern Hemisphere circulation variability [*Ding and Wang, 2005*]. It is possible that the CGT may influence Northern Hemisphere heat waves in some way; however, we find no evidence connecting May BSISO propagation to Plains August heat waves though the CGT. Finally, we found some evidence suggesting that the teleconnection may be modulated by the El Niño Southern Oscillation, operating primarily in El Niño-decaying years.

This study demonstrates that a weather anomaly in the tropical Western Pacific can be used to forecast US Plains heat waves at three-month lead times with more skill than current seasonal forecasts [*Luo and Zhang*, 2012], thus allowing more time for preparation.

REFERENCES

Barnston, A. G. (1994), Linear statistical short-term climate predictive skill in the Northern Hemisphere, *J. Clim.*, *7*(10), 1513–1564, doi:10.1175/1520-0442(1994)007<1513:LSSTCP>2.0.CO;2.

Chen, M., et al. (2008), CPC Unified gauge-based analysis of global daily precipitation, paper presented Western Pacific Geophysics Meeting, Cairns, Austraila, 29 July-1 Aug.

Ding, Q., and B.Wang (2005), Circumglobal teleconnection in the northern hemisphere summer, *J. Clim., 18*(17), 3483–3505, doi:10.1175/JCLI3473.1

Donald, A., H. Meinke, B. Power, A. d. H. N. Maia, M. C. Wheeler, N. White, R. C. Stone, and J. Ribbe (2006), Near-global impact of the Madden-Julian Oscillation on rainfall, *Geophys. Res. Lett.*, *33*(9), 1–4, doi:10.1029/2005GL025155.

Drosdowsky, W., and L. E. Chambers (2001), Near-global sea surface temperature anomalies as predictors of Australian seasonal rainfall, *J. Clim.*, *14*(7), 1677–1687, doi:10.1175/1520-0442(2001)014<1677:NACNGS>2.0.CO;2.

Duerinck, H. M., R. J. van der Ent, N. C. van de Giesen, G. Schoups, V. Babovic, and P. J.-F. Yeh (2016), Observed soil moisture-precipitation feedback in Illinois: A systematic analysis over different scales, *J. Hydrometeor.*, 1645–1660, doi:10.1175/JHM-D-15-0032.1.

Eltahir, E. a. B. (1998), A soil moisture-rainfall feedback mechanism: 1. Theory and observations, *Water Resour. Res.*, *34*(4), 765–776, doi:10.1029/97WR03499.

Ferranti, L., T. N. Palmer, F. Molteni, and E. Klinker (1990), Tropical-extratropical interaction associated with the 30-60 day oscillation and its impact on medium and extended range prediction, *J. Atmos. Sci.*, *47*(18), 2177–2199, doi:10.1175/1520- 0469(1990)047<2177:TEIAWT>2.0.CO;2.

Frankignoul, C., and N. Sennéchael (2007), Observed influence of North Pacific SST anomalies on the atmospheric circulation, *J. Clim.*, *20*(3), 592–606, doi:10.1175/JCLI4021.1.

Hoskins, B. J., and D. J. Karoly (1981), The steady linear response of a spherical atmosphere to thermal and orographic forcing, *J. Atmos. Sci.*, *38*(6), 1179–1196, doi:10.1175/1520-0469(1981)038<1179:TSLROA>2.0.CO;2.

Kalnay, E., M. Kanamitsu, R. Kistler, W. Collins, D. Deaven, L. Gandin, M. Iredell, S. Saha, G. White, J. Woollen, Y. Zhu, M. Chelliah, W. Ebisuzaki, W. Higgins, J. Janowiak, K. C. Mo, C. Ropelewski, J. Wang, A. Leetmaa, R. Reynolds, R. Jenne, and D. Joseph (1996), The NCEP/NCAR 40-year reanalysis project, *Bull. Am. Meteorol. Soc.*, *77*(3), 437–471, doi:10.1175/1520-0477(1996)077<0437:TNYRP>2.0.CO;2.

Kanamitsu, M., W. Ebisuzaki, J. Woollen, S. K. Yang, J. J. Hnilo, M. Fiorino, and G. L. Potter (2002), NCEP-DOE AMIP-II reanalysis (R-2), *Bull. Am. Meteorol. Soc.*, *83*(11), 1631–1643, doi:10.1175/BAMS-83-11-1631.

Kemball-Cook, S., and B. Wang (2001), Equatorial waves and airâA˘Ssea interaction in the boreal summer intraseasonal oscillation, *J. Clim.*, *14*(13), 2923–2942, doi:10.1175/1520- 0442(2001)014<2923:EWAASI>2.0.CO;2.

Koster, R. D., P. A. Dirmeter, Z. Guo, G. Bonan, E. Chan, P. Cox, C. Gordon, S. Kanae, E. Kowalczyk, D. Lawrence, P. Liu, C.-H. Lu, S. Malyshev, B. McAvaney, K. Mitchell, D. Mocko, T. Oki, K. Oleson, A. Pitman, Y. Sud, C. M. Taylor, D. Verseghy, R. Vasic, Y. Xue, and T. Yamada (2004), Regions of strong coupling between soil moisture and precipitation, *Science*, *305*(5687), 1138–1140, doi:10.1126/science.1100217.

Lau, K.-M., and P. H. Chan (1986), Aspects of the 40-50 day oscillation during the northern summer as inferred from outgoing longwave radiation, *Mon. Weather Rev.*, *114*(7), 1354–1367, doi:10.1175/1520-0493(1986)114<1354:AOTDOD>2.0.CO;2.

Lee, J. Y., B. Wang, M. C. Wheeler, X. Fu, D. E. Waliser, and I. S. Kang (2013), Real-time multivariate indices for the boreal summer intraseasonal oscillation over the Asian summer monsoon region, *Clim. Dynam.*, *40*(1-2), 493–509, doi:10.1007/s00382-012- 1544-4.

Liebmann, B., and C. A. Smith (1996), Description of a complete (interpolated) outgoing longwave radiation dataset, *Bull. Am. Meteorol. Soc.*, *77*(6), 1275–1277.

Lin, A., and T. Li (2008), Energy spectrum characteristics of boreal summer intraseasonal oscillations: Climatology and variations during the ENSO developing and decaying phases, *J. Clim.*, *21*(23), 6304–6320, doi:10.1175/2008JCLI2331.1.

Liu, Q., N. Wen, and Z. Liu (2006), An observational study of the impact of the North Pacific SST on the atmosphere, *Geophys. Res. Lett.*, *33*(18), doi:10.1029/2006GL026082.

Luo, L., and Y. Zhang (2012), Did we see the 2011 summer heat wave coming?, *Geophys. Res. Lett.*, *39*(9), 1–5, doi:10.1029/2012GL051383.

McKee, T. B., N. J. Doesken, and J. Kleist (1993), The relationship of drought frequency and duration to timescales, paper presented at 8th Conference on Applied Climatology, Am. Meteorol. Soc., Anaheim, Calif.

McKinnon, K. A., A. Rhines, M. P. Tingley, and P. Huybers (2016), Long-lead predictions of eastern United States hot days from Pacific sea surface temperatures, *Nat. Geosci.*, *9*(5), 389–396, doi:10.1038/NGEO2687.

Melillo, J. M., T. C. Richmond, and G. W. Yohe (Eds.) (2014), Climate change impacts in the United States: The third national climate assessment, 841 pp., *U.S. Global Change Research Program*, Washington, D. C., doi:10.7930/J0Z31WJ2.

Menne, M. J., I. Durre, R. S. Vose, B. E. Gleason, and T. G. Houston (2012), An overview of the global historical climatology network-daily database, *J. Atmos. Oceanic Technol.*, *29*(7), 897–910, doi:10.1175/JTECH-D-11-00103.1.

Moon, J. Y., B. Wang, K. J. Ha, and J. Y. Lee (2013), Teleconnections associated with Northern Hemisphere summer monsoon intraseasonal oscillation, *Clim. Dynam.*, *40*(11), 2761–2774, doi:10.1007/s00382-012-1394-0.

Namias, J. (1982), Anatomy of Great Plains protracted heat waves (especially the 1980 U.S. summer drought), *Mon. Weather Rev.*, *110*(7), 824–838, doi:10.1175/1520-0493(1982)110<0824:AOGPPH>2.0.CO;2.

Newman, M., and P. D. Sardeshmukh (1998), The impact of the annual cycle on the North Pacific/North American response to remote low-frequency forcing, *J. Atmos. Sci.*, *55*(8), 1336–1353, doi:10.1175/1520-0469(1998)055<1336:TIOTAC>2.0.CO;2.

Pepler, A. S., L. B. Díaz, C. Prodhomme, F. J. Doblas-Reyes, and A. Kumar (2015), The ability of a multi-model seasonal forecasting ensemble to forecast the frequency of warm, cold and wet extremes, *Weather Clim. Extrem.*, *9*, 68–77, doi:10.1016/j.wace.2015.06.005.

Portier, C., K. Thigpen Tart, S. Carter, C. Dilworth, A. Grambsch, J. Gohlke, J. Hess, S. Howard, G. Luber, J. Lutz, T. Maslak, M. Radtke, J. Rosenthal, T. Rowles, P. Sandifer, J. Scheraga, D. Strickman, J. Trtanj, and P.-Y. Whung (2010), A human health perspective on climate change: A report outlining research needs on the human health effects of climate change, 80 pp., *Environmental Health Perspectives/National Institute of Environmental Health Sciences*, Triangle Park, N. C., doi:10.1289/ehp.1002272.

Ropelewski, C. F., and M. S. Halpert (1987), Global and regional scale precipitation pat- terns associated with the El Niño/Southern Oscillation, *Mon. Weather Rev.*, *115*(8), 1606–1626, doi:10.1175/1520-0493(1987)115<1606:GARSPP>2.0.CO;2.

Slade, S. A., and E. D. Maloney (2013), An intraseasonal prediction model of Atlantic and East Pacific tropical cyclone genesis, *Mon. Weather Rev.*, *141*(6), 1925–1942, doi:10.1175/MWR-D-12-00268.1.

Teng, H., and B. Wang (2003), Interannual variations of the boreal summer intraseasonal oscillation in the Asian-Pacific Region*, *J. Clim.*, *16*(22), 3572–3584, doi:10.1175/1520- 0442(2003)016<3572:IVOTBS>2.0.CO;2.

Trenberth, K. E. (1997), The definition of El Niño, *Bull. Am. Meteorol. Soc.*, *78*(12), 2771–2777, doi:10.1175/1520-0477(1997)078<2771:TDOENO>2.0.CO;2.

Wang, B., and H. Rui (1990), Synoptic climatology of transient tropical intraseasonal convection anomalies: 1975-1985, *Meteorol. Atmos. Phys.*, *44*(1), 43–61, doi:10.1007/BF01026810.

Wang, B., and X. Xie (1997), A Model for the boreal summer intraseasonal oscillation, *J. Atmos. Sci.*, *54*(1), 72–86, doi:10.1175/1520-0469(1997)054<0072:AMFTBS>2.0.CO;2.

Wheeler, M. C., and H. H. Hendon (2004), An all-season real-time multivariate MJO index: Development of an index for monitoring and prediction, *Mon. Weather Rev.*, *132*(8), 1917–1932, doi:10.1175/1520-0493(2004)132<1917:AARMMI>2.0.CO;2.

Yasunari, T. (1979), Cloudiness fluctuations associated with the northern hemisphere summer monsoon, *J. Meteor. Soc. Japan*, *57*(3), 227–242.

APPENDIX A: SUPPLEMENTARY FIGURES

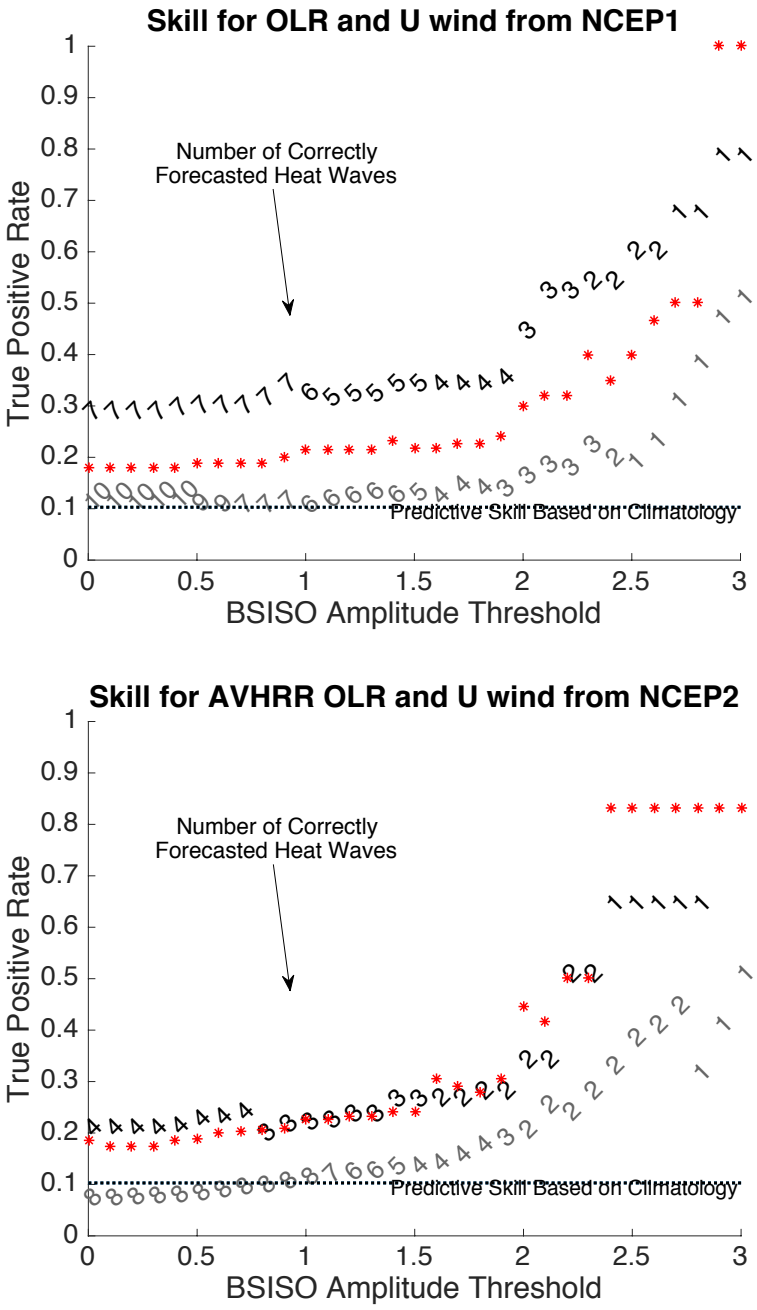

Figure A.1: Comparison of forecast skill between BSISO indices created using different datasets for years 1983 to 2013. Top panel: Outgoing longwave radiation (OLR) and zonal wind at 850 hPa (U) from the NCEP/NCAR Reanalysis 1 product. Bottom panel: OLR from Advanced Very High Resolution Radiometer (AVHRR) satellite product and U from NCEP/DOE Reanalysis 2 product. See Figure 2 for formatting information.

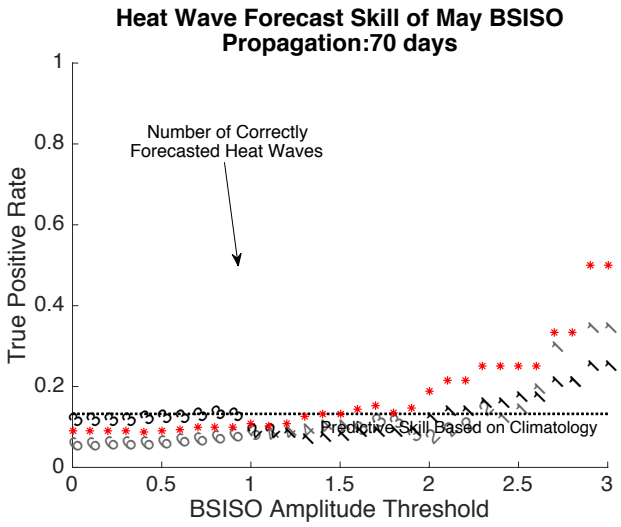
Heat Wave Forecast Skill of May BSISO
Propagation:70 days
Number of Correctly
Forecasted Heat Waves
Predictive Skill Based on Climatology
True Positive Rate
BSISO Amplitude Threshold

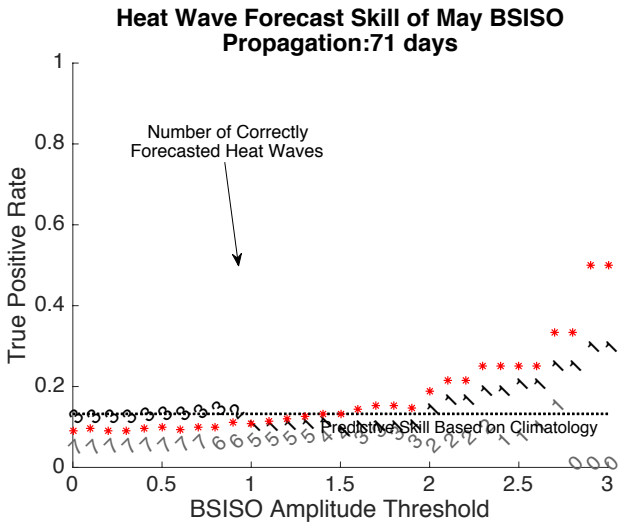
Heat Wave Forecast Skill of May BSISO
Propagation:71 days
Number of Correctly
Forecasted Heat Waves
Predictive Skill Based on Climatology
True Positive Rate
BSISO Amplitude Threshold

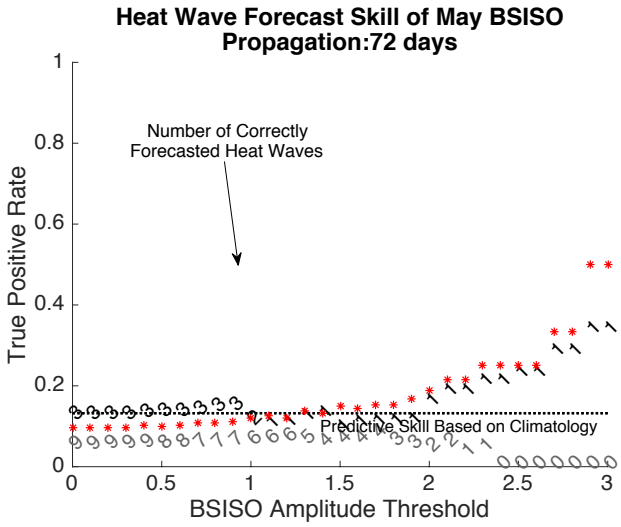
Heat Wave Forecast Skill of May BSISO
Propagation:72 days
Number of Correctly
Forecasted Heat Waves
Predictive Skill Based on Climatology
True Positive Rate
BSISO Amplitude Threshold

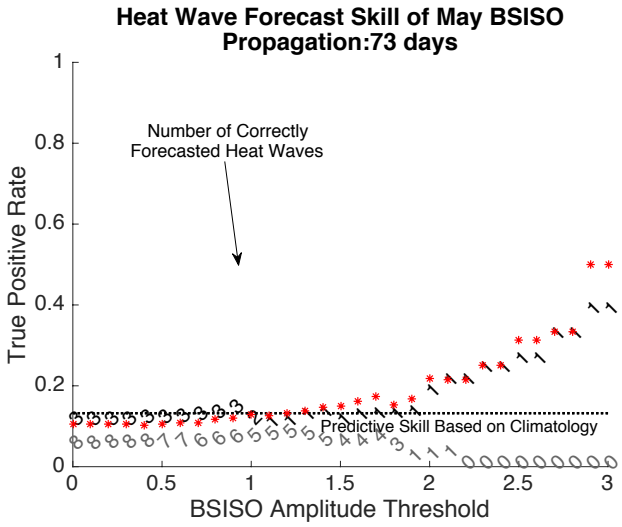
Heat Wave Forecast Skill of May BSISO
Propagation:73 days
Number of Correctly
Forecasted Heat Waves
Predictive Skill Based on Climatology
True Positive Rate
BSISO Amplitude Threshold

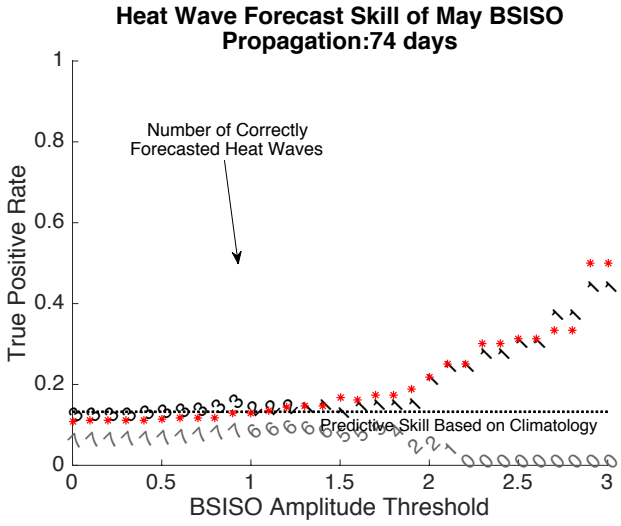
Heat Wave Forecast Skill of May BSISO
Propagation:74 days
Number of Correctly
Forecasted Heat Waves
Predictive Skill Based on Climatology
True Positive Rate
BSISO Amplitude Threshold

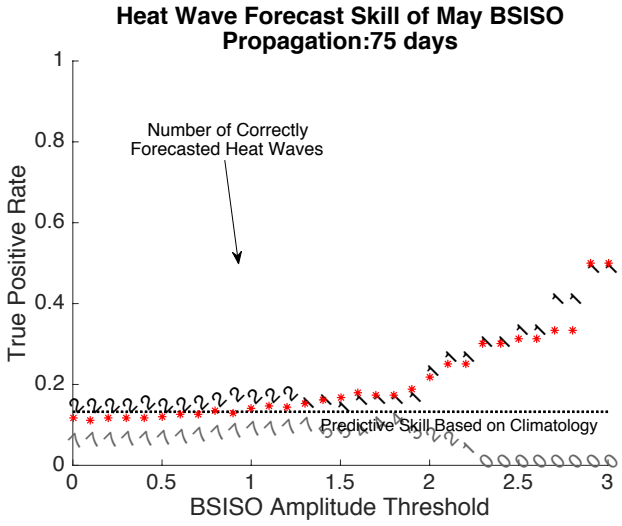
Heat Wave Forecast Skill of May BSISO
Propagation:75 days
Number of Correctly
Forecasted Heat Waves
Predictive Skill Based on Climatology
True Positive Rate
BSISO Amplitude Threshold

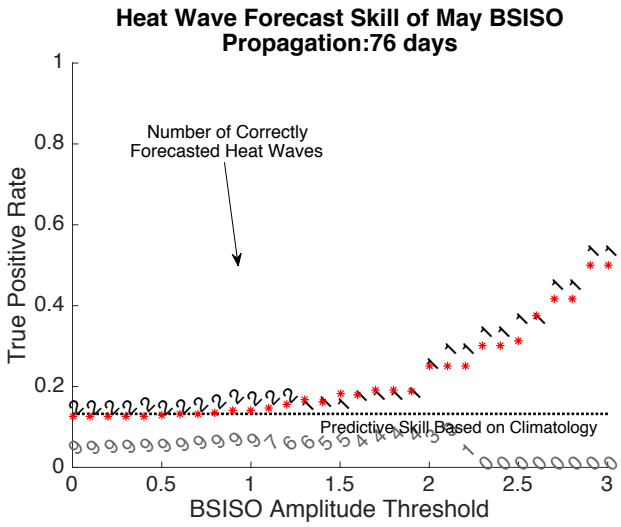
Heat Wave Forecast Skill of May BSISO
Propagation:76 days
Number of Correctly
Forecasted Heat Waves
Predictive Skill Based on Climatology
True Positive Rate
BSISO Amplitude Threshold

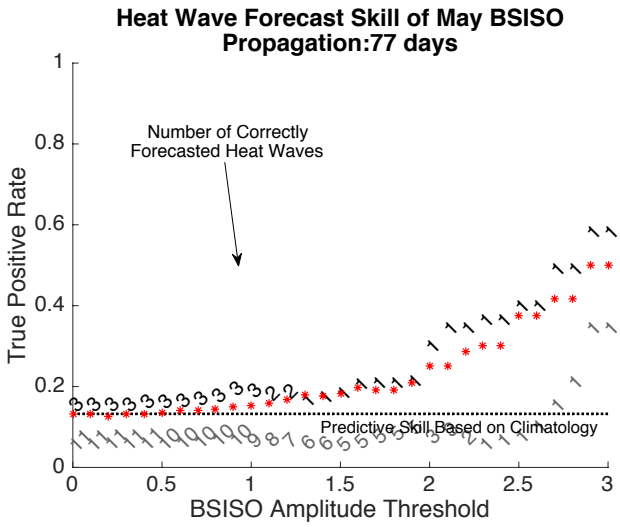
Heat Wave Forecast Skill of May BSISO
Propagation:77 days
Number of Correctly
Forecasted Heat Waves
Predictive Skill Based on Climatology
True Positive Rate
BSISO Amplitude Threshold

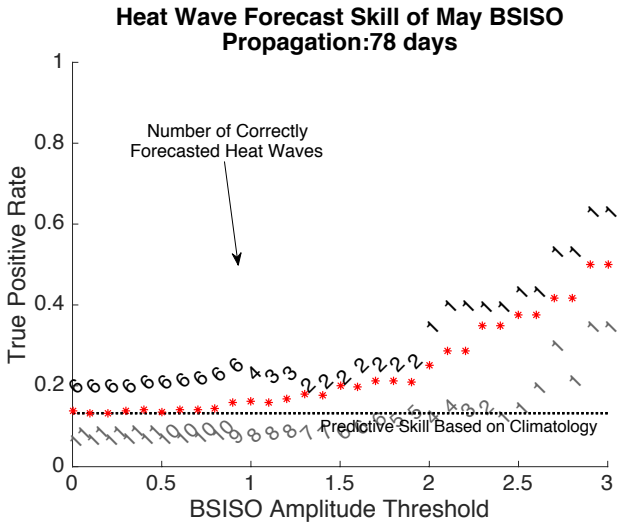
Heat Wave Forecast Skill of May BSISO
Propagation:78 days
Number of Correctly
Forecasted Heat Waves
Predictive Skill Based on Climatology
True Positive Rate
BSISO Amplitude Threshold

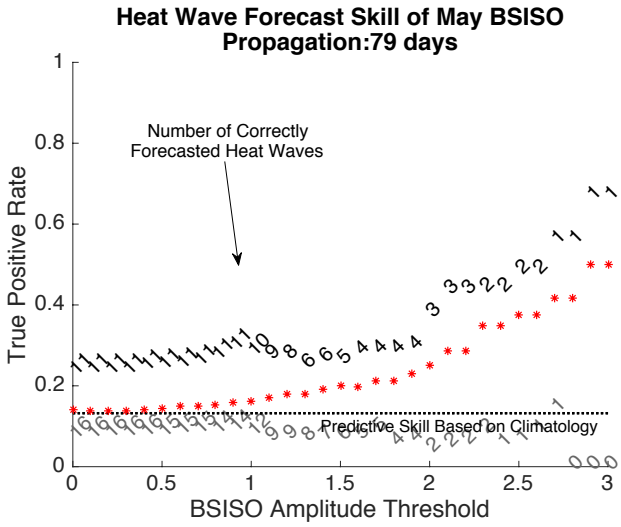
Heat Wave Forecast Skill of May BSISO
Propagation:79 days
Number of Correctly
Forecasted Heat Waves
Predictive Skill Based on Climatology
True Positive Rate
BSISO Amplitude Threshold

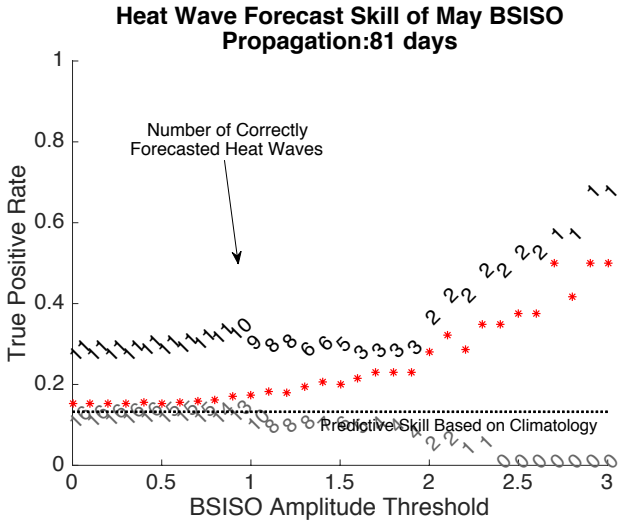
Heat Wave Forecast Skill of May BSISO
Propagation:81 days
Number of Correctly
Forecasted Heat Waves
Predictive Skill Based on Climatology
True Positive Rate
BSISO Amplitude Threshold

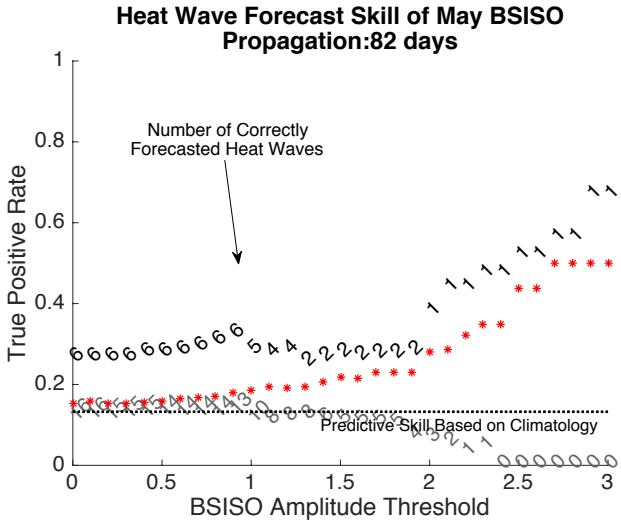
Heat Wave Forecast Skill of May BSISO
Propagation:82 days
Number of Correctly
Forecasted Heat Waves
Predictive Skill Based on Climatology
True Positive Rate
BSISO Amplitude Threshold

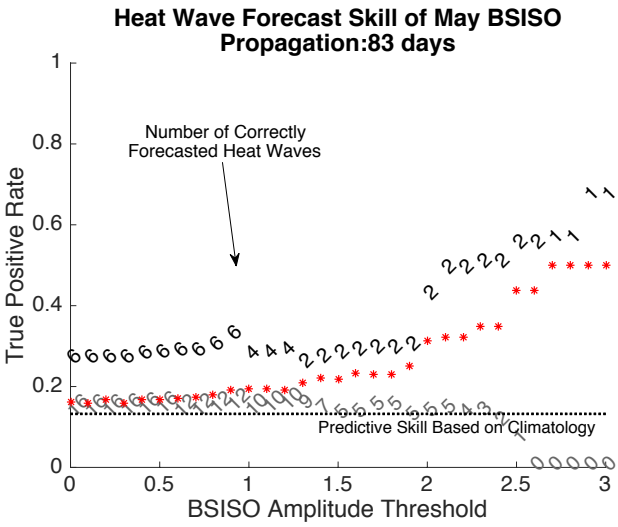
Heat Wave Forecast Skill of May BSISO
Propagation:83 days
Number of Correctly
Forecasted Heat Waves
Predictive Skill Based on Climatology
True Positive Rate
BSISO Amplitude Threshold

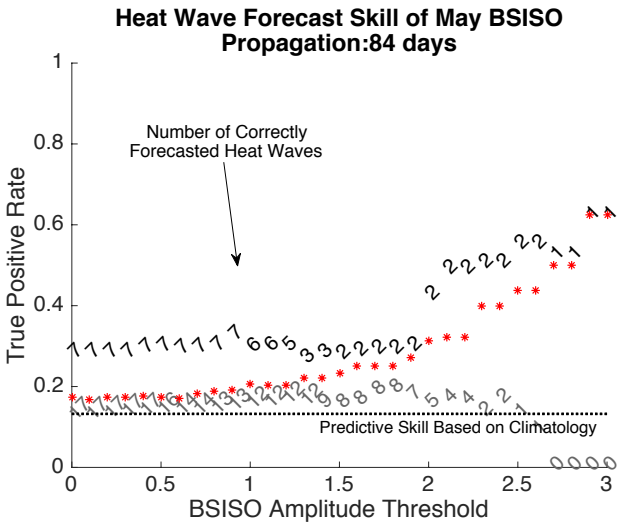
Heat Wave Forecast Skill of May BSISO
Propagation:84 days
Number of Correctly
Forecasted Heat Waves
Predictive Skill Based on Climatology
True Positive Rate
BSISO Amplitude Threshold

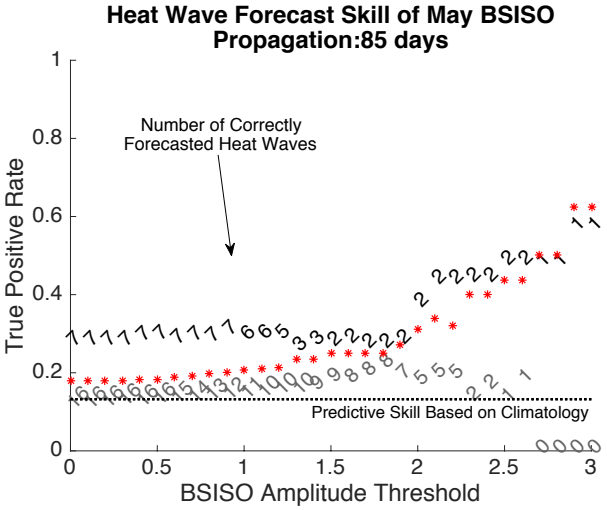
Heat Wave Forecast Skill of May BSISO
Propagation:85 days
Number of Correctly
Forecasted Heat Waves
Predictive Skill Based on Climatology
True Positive Rate
BSISO Amplitude Threshold

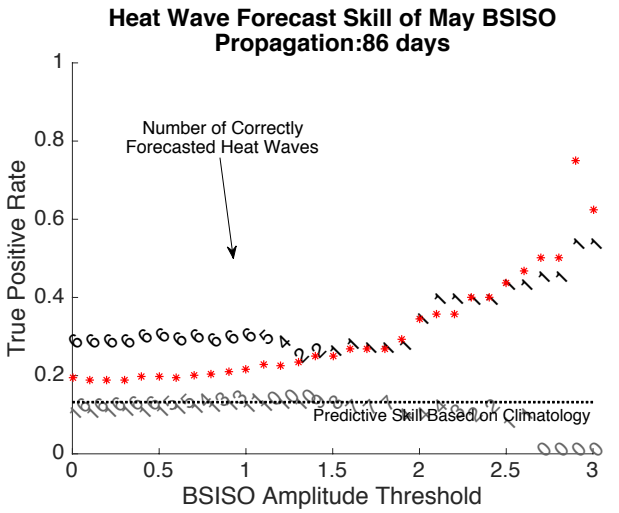
Heat Wave Forecast Skill of May BSISO
Propagation:86 days
Number of Correctly
Forecasted Heat Waves
Predictive Skill Based on Climatology
True Positive Rate
BSISO Amplitude Threshold

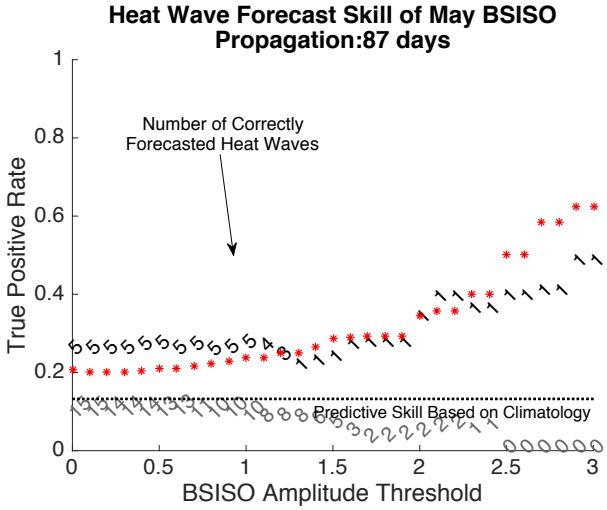
Heat Wave Forecast Skill of May BSISO
Propagation:87 days
Number of Correctly
Forecasted Heat Waves
Predictive Skill Based on Climatology
True Positive Rate
BSISO Amplitude Threshold

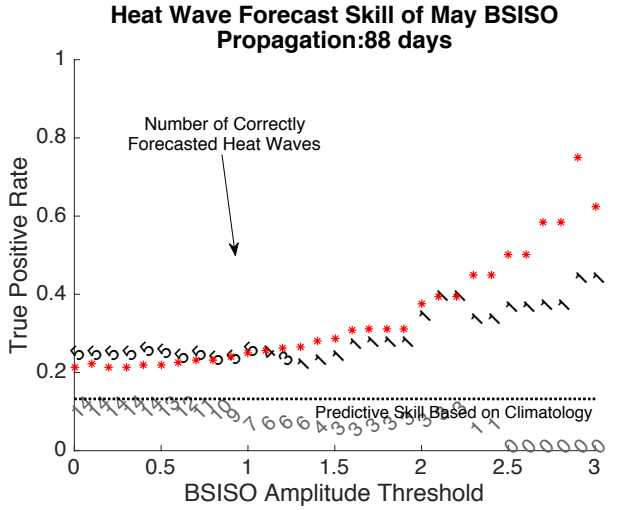
Heat Wave Forecast Skill of May BSISO
Propagation:88 days
Number of Correctly
Forecasted Heat Waves
Predictive Skill Based on Climatology
True Positive Rate
BSISO Amplitude Threshold

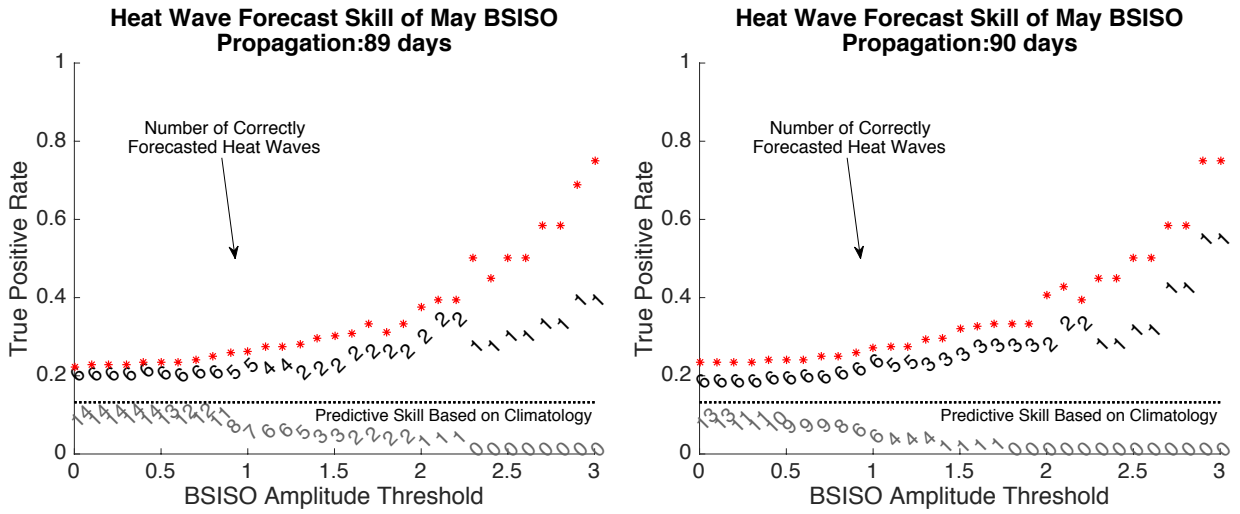

Figure A.2: Heat wave forecast skill at lead times between 70 and 90 days. Skill for 80 days has been omitted here, because it is shown in Figure 2. See Figure 2 for formatting information.

Table A.1: August Plains heat wave events correctly forecasted at lead times between 70 and 90 days. An 'x' denotes a correct forecast.

Lead Time ➔ / Heat Wave ➘	70	71	72	73	74	75	76	77	78	79	80	81	82	83	84	85	86	87	88	89	90
18-19 August 1948										x	x			x	x	x	x	x	x	x	x
22-30 August 1948					x	x	x	x	x	x	x	x	x	x	x	x	x	x	x		
12-13 August 1955	x	x								x	x	x			x	x	x	x	x	x	
7-9 August 1958											x		x							x	x
6-8 August 1978									x	x	x	x		x	x	x	x				
16-21 August 1983			x	x				x	x	x	x	x	x				x	x	x	x	x
14-19 August 1988	x	x	x	x	x				x	x	x	x	x	x	x	x					
15-17 August 1990									x	x	x	x	x								x
6-7 August 1995										x	x	x								x	x
23-24 August 1997										x	x	x		x	x	x					
14-27 August 2003	x	x	x	x	x	x	x	x	x	x	x	x	x	x	x	x	x	x	x	x	x
15-16 August 2007										x	x	x									

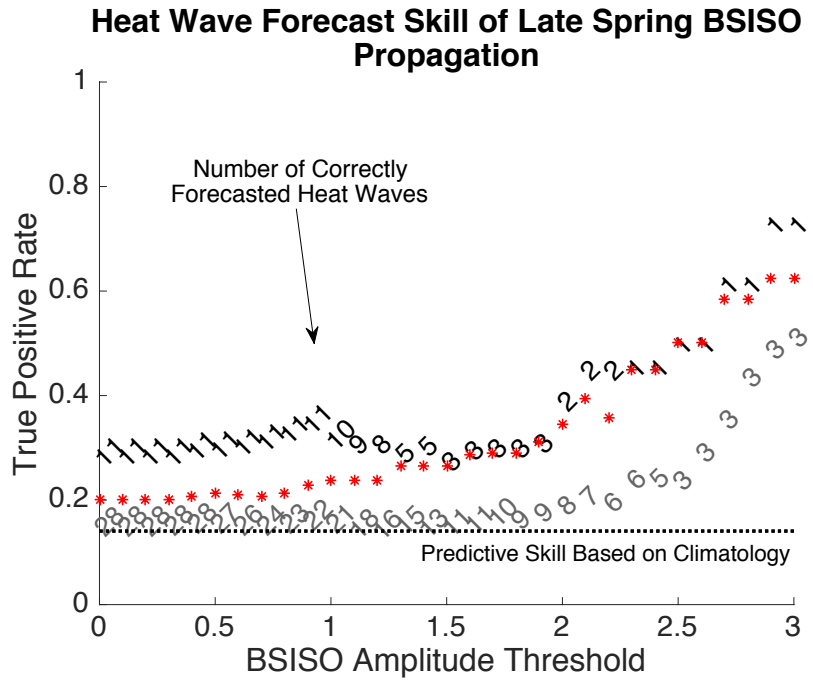

Figure A.3: Same as Figure 2, but now heat waves are defined as occurring when at least 20% of the Plains experiences a daily maximum temperature above 35°C (95°F).

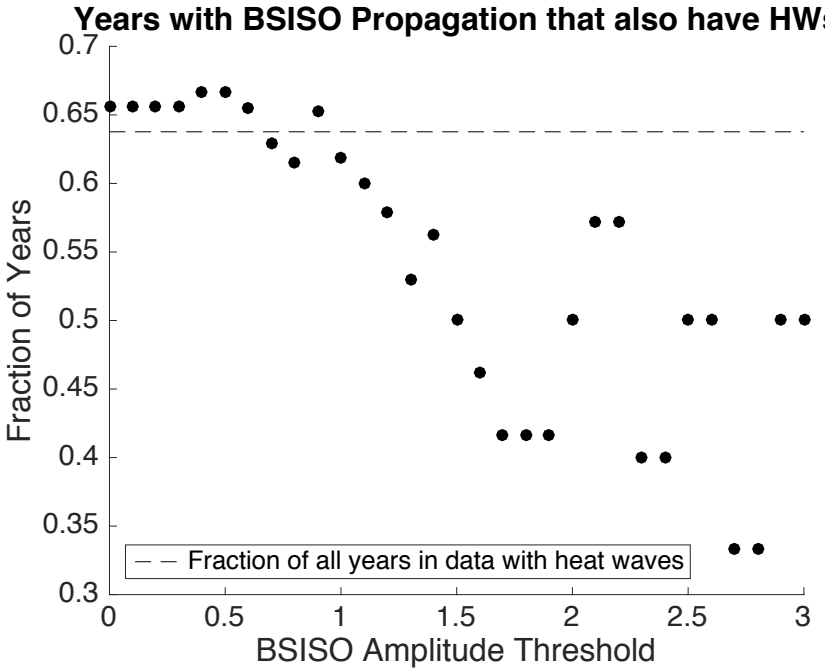

Figure A.4: Fraction of years that have BSISO propagation, that also have August heat waves in the Plains (scatter points). Fraction of all years (1948-2016) with heat waves (dashed line).

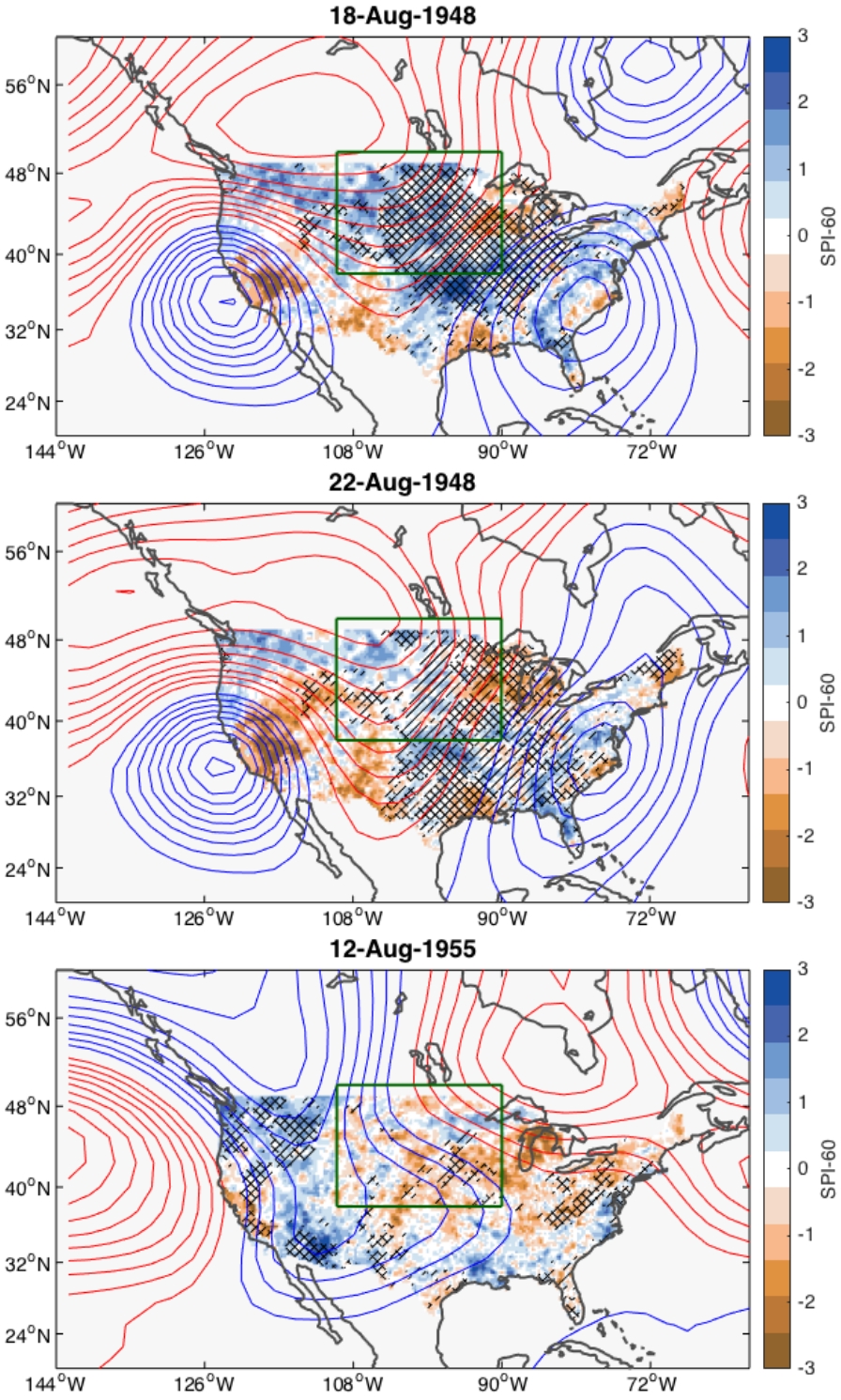
18-Aug-1948
22-Aug-1948
12-Aug-1955
56°N
48°N
40°N
32°N
24°N
144°W
126°W
108°W
90°W
72°W
SPI-60
3
2
1
0
-1
-2
-3

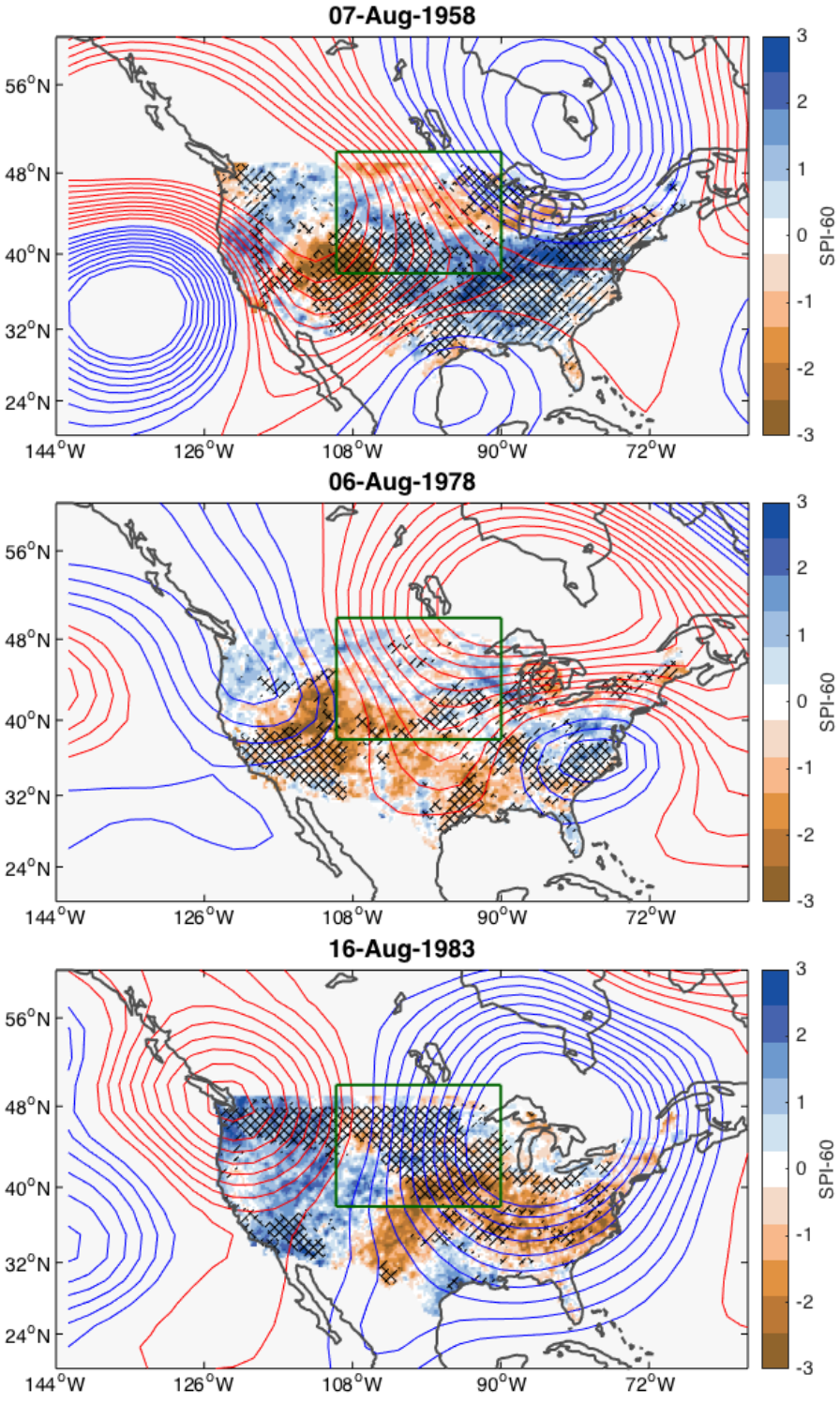
07-Aug-1958
06-Aug-1978
16-Aug-1983
56°N
48°N
40°N
32°N
24°N
144°W
126°W
108°W
90°W
72°W
SPI-60
3
2
1
0
-1
-2
-3

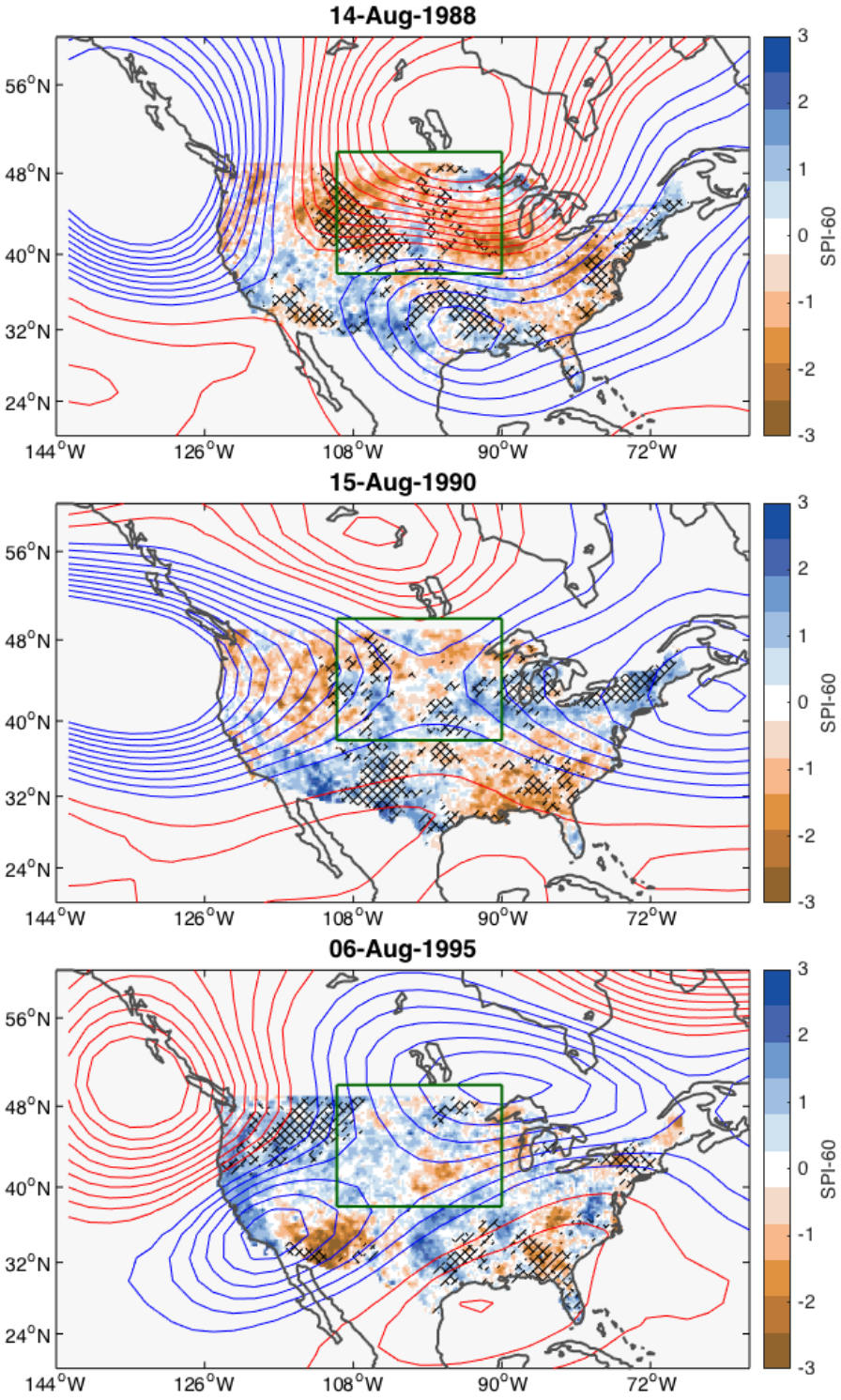
14-Aug-1988
15-Aug-1990
06-Aug-1995
56°N
48°N
40°N
32°N
24°N
144°W
126°W
108°W
90°W
72°W
SPI-60
3
2
1
0
-1
-2
-3

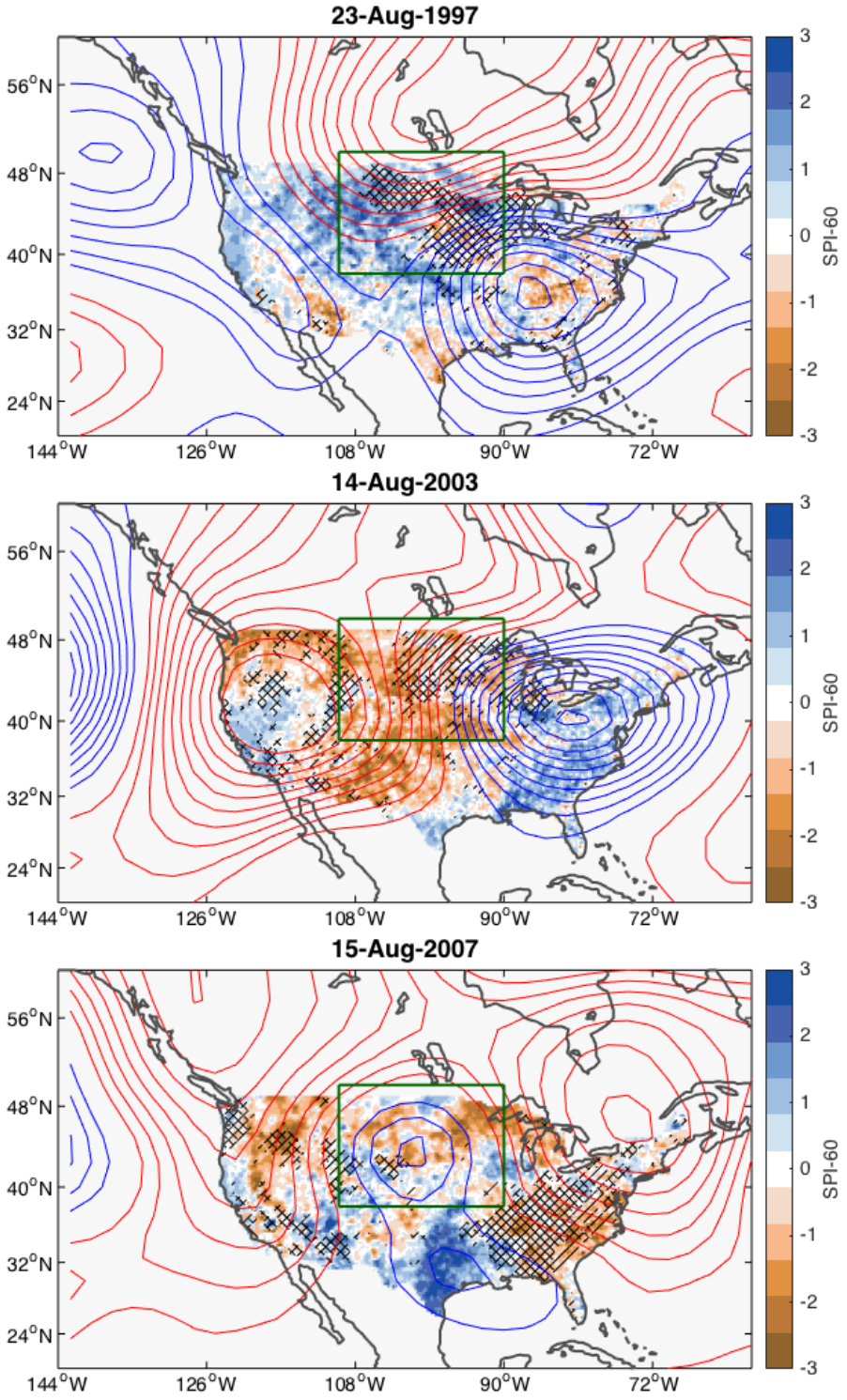

Figure A.5: As in Figure 5, but for individual correctly forecasted heat wave events. Note the different scale for SPI-60. Geopotential height anomalies at 500 hPa are now in increments in 10m, beginning at 10m.